Simulation of the interaction between Fe impurities and point defects in V

Mikhail I. Mendelev
Materials and Engineering Physics, Ames Laboratory, Ames, Iowa 50011, USA

Seungwu Han
Department of Physics, Ewha Womans University, Seoul 120-750, Korea

Won-joon Son
School of Chemistry, Seoul National University, Seoul 151-742, Korea

Graeme J. Ackland
School of Physics, University of Edinburgh, Edinburgh EH9 3JZ, Scotland, United Kingdom

David J. Srolovitz
Department of Physics, Yeshiva University, New York, New York 10033, USA
(Received 19 June 2007; published 11 December 2007)

We report improved results of atomistic modeling of V-Fe alloys. We introduced an electronic structure embedding approach to improve the description of the point defects in first-principles calculations, by including the semicore electrons in some V atoms (those near the interstitial where the semicore levels are broadened) but not those further from the point defect. This enables us to combine good accuracy for the defect within large supercells and to expand the data set of first-principles point defect calculations in vanadium with and without small amounts of iron. Based on these data, previous first-principles work, and new calculations on the alloy liquid, we fitted an interatomic potential for the V-Fe system which describes the important configurations likely to arise when such alloys are exposed to radiation. This potential is in a form suitable for molecular dynamics (MD) simulations of large systems. Using the potential, we have calculated the migration barriers of vacancies in the presence of iron, showing that these are broadly similar. On the other hand, MD simulations show that V self-diffusion at high temperatures and Fe diffusion are greatly enhanced by the presence of interstitials.

DOI: 10.1103/PhysRevB.76.214105 PACS number(s): 61.72.−y, 34.20.Cf, 66.30.Fq, 61.80.−x

I. INTRODUCTION

Future fusion reactors will require advanced materials to cope with high temperatures, neutron irradiation, and contact with liquid lithium. Although long industrial experience with steel makes it the current material of choice, the costs of replacing fusion reactor components makes longer-lived materials especially attractive as structural blanket materials. Vanadium-based alloys[1–13] such as VCrTi are an attractive possibility on account of their good high-temperature strength and absence of radioactive products in a 14 MeV neutron flux. Swelling of materials, from void or vacancy trapping in the bulk, is one of the limiting features in such radiation environments, and one of the largest swelling materials reported is V-Fe.[14–17] It is of interest to understand which properties of this material are responsible for the swelling.

Experience shows that the behavior of pure materials under irradiation can be radically altered by even small quantities of alloying elements. One such dramatic case is that of iron or chromium which, in small quantities, can radically increase the rate of swelling of vanadium. Since swelling can produce large stresses, it is important to identify the mechanisms behind such effects. Molecular dynamics (MD) is the method of choice for studying damage caused by neutron irradiation. The strong correlation between atomic size and vulnerability to swelling in vanadium alloys suggests that molecular dynamics provides a reasonable approach for exploring this mechanism. The relatively short time scale of damage cascade formation means that following atom trajectories in reasonable simulation time is possible, and the likely importance of crystal defects advocates for the employment of an off-lattice simulation method. Reasonable atomistic simulations require descriptions of the interaction between atoms that yield reasonable properties for the material of interest. Interatomic potentials of the embedded atom method[18] (EAM) or Finnis-Sinclair[19] (FS) form are widely used to describe metals because they provide an excellent tradeoff between computational speed and accurate reproduction of key materials properties. For example, such potentials can accurately describe atomic size, elastic strain, the effects of change in atomic coordination around vacancies and interstitials, etc.

We have previously performed first-principles calculations and constructed interatomic potentials for pure vanadium[20] and for pure iron,[21] which accurately reproduce many perfect crystal and crystal defect properties. In general, defect formation energies can be predicted reliably only by first-principles methods, and not by the embedded atom method; however, if these energies are fitted, simulation using the embedded atom method can give a reliable description of their interactions and assembly into voids or dislocation loops.

TABLE I. Physical properties of V calculated using FS potentials (The properties used in the fitting procedure are printed in bold.)

Property	Target value	Potential from Ref. 20	New potential
a (bcc) (Å)	3.039 (Ref. 37)	**3.030**	**3.030**
E_{coh} (bcc) (eV/atom)	−5.31 (Ref. 38)	**−5.300**	−5.016
C_{11} (GPa)	229 (Ref. 39)	**228**	**228**
C_{12} (GPa)	119 (39)	**119**	**119**
C_{44} (GPa)	43 (Ref. 39)	**4.3**	**42**
E_f^{vac} (unrelaxed bcc) (eV/atom)	2.91 (Ref. 40)	**2.91**	2.75
E_f^{vac} (relaxed bcc) (eV/atom)	2.48 (Ref. 40)	2.62	**2.49**
E_m^{vac} (bcc) (eV/atom)		0.52	0.78
E_D (bcc) (eV/atom) ($E_f^{vac}+E_m^{vac}$)	3.19 (Ref. 41 and 42) 4.08 (Ref. 41 and 43)	3.14	3.27
E_f^i (bcc ⟨100⟩) (eV/atom)	3.22 (Ref. 40)	***3.540*** (Ref. 45)	**3.21**
E_f^i (bcc ⟨110⟩) (eV/atom)	3.09 (Ref. 40)	***3.739***	**3.09**
E_f^i (bcc ⟨111⟩) (eV/atom)	2.81 (Ref. 40)	***3.280***	**2.81**
E_f^i (bcc crowdion) (eV/atom)	2.81 (Ref. 40)	***3.300***	**2.83**
E_f^i (bcc octahedral) (eV/atom)	3.27 (Ref. 40)	***4.266***	**3.24**
$d_{\langle 100\rangle}$ (Å)	2.170 (Ref. 40)	2.106	2.022
$d_{\langle 110\rangle}$ (Å)	2.108 (Ref. 40)	2.186	2.224
$d_{\langle 111\rangle}$ (Å)	2.151 (Ref. 40)	2.238	2.192
a (fcc) (A)	3.861 (Ref. 40)	3.947	**3.863**
$\Delta E_{bcc\rightarrow fcc}$ (eV/atom)	0.247 (Ref. 40)	0.158	**0.214**
T_m (K)	2183 (Ref. 44)	2924	3119

In this paper we present further first-principles data on self-interstitials in V and Fe impurities in V. We also present a semiempirical potential that reproduces the main first-principles results. The potential has an analytic many-body form, making it suitable for application in existing large-scale MD codes. Using this semiempirical potential, we have studied vacancy and interstitial diffusion in V in the presence of Fe impurities.

II. FIRST-PRINCIPLES CALCULATIONS

All first-principles calculations were carried out using the density functional theory and plane-wave pseudopotential methods with the exchange-correlation potential described by the generalized gradient approximation,[22] which is required to get the correct magnetic moment for iron. In all static simulations the atomic positions were relaxed according to the Hellmann-Feynman forces and the unit cell relaxed according to the stresses. For a consistency check, we have used both VASP (Ref. 23) and PWSCF (Ref. 24) codes in the smaller simulations, and, as has been demonstrated previously, the results agree. The energy cutoff of 40 Ry was used to expand the plane wave basis. For the conventional unit cell of V or Fe, $8\times8\times8$ k-point mesh was used while equivalent densities were chosen for supercell structures.

We have generated two pseudopotentials for vanadium.[25] One includes semicore states ($3s3p$) as valence electrons, while the other treats them as part of the frozen core. We apply the pseudopotential including semicore states to atoms when the bond length between them is compressed by more than 10% compared to the bond length in a perfect vanadium crystal at zero pressure. The improved transferrability of the semicore pseudopotential ensures the computational accuracy, while the high computational cost associated with calculating semicore states is avoided, since relatively few bonds are sufficiently compressed to meet the 10% compression condition (e.g., in the vicinity of self-interstitials). For Fe, the same pseudopotential, including semicore states, is used throughout.

Since only nonsemicore potentials were used in Ref. 20, in the present study we recalculated the self-interstitial formation energies in pure V. The new values presented in Table I are slightly smaller than those reported in Ref. 20 but the relative differences between intersitital configurations agree well with previous results (to within 0.05 eV).

We considered several V-Fe compound structures that are based on the bcc structure—$V_{15}Fe$, VFe, VFe_{15}. We considered VFe in the CsCl structure. For $V_{15}Fe$ and VFe_{15}, we replaced one of the atoms in $2\times2\times2$ bcc supercell with the counterpart atom. We then calculated the lattice parameters and formation energies for each of these systems. The results are presented in Table II.

The vacancy-Fe interaction energy can be defined as

$$\Delta E_{\text{vac-Fe}} = E_{\text{vac}}[1\text{Fe}] + E_p[0\text{Fe}] - E_{\text{vac}}[0\text{Fe}] - E_p[1\text{Fe}], \tag{1}$$

where $E_p[n\text{Fe}]$ is the energy of a system containing N body-centered-cubic lattice sites of which n sites are occupied by Fe atoms, and $E_{\text{vac}}[n\text{Fe}]$ is the energy of a system containing

TABLE II. The properties of V-Fe alloys obtained from the first-principles calculations and with the new FS potential. The propertial. The properties used in the fitting procedure are printed in bold. a is the lattice parameter of the supercell with two or 16 atoms, $\Delta E_{i\text{-Fe}}^{\langle 100\rangle}$ is the interstitial-Fe interaction energy and $\Delta E_{\text{vac-Fe}}$ (eV) is the vacncy-Fe interaction energy. As we see. the iron is bound to the various interstitials but repelled by the vacncy. The strong binding of Fe in the $\langle 110\rangle$ mixed interstitial conformation brings it to within 0.07 eV of that of the $\langle 111\rangle$ mixed interstitial.

Property	First principles	FS potential
a (V bcc) (Å)	3.030(Ref.46)	**3.030**
a (Fe bcc) (Å)	2.855	**2.855**
a ($V_{15}Fe$) (Å)	6.005	**6.007**
a (VFe) (Å)	2.903	2.968
a (VFe_{15})	5.726	5.758
$\Delta E_{i\text{-Fe}}^{\langle 100\rangle}$ (eV)	−0.02	**−0.03**
$\Delta E_{i\text{-Fe}}^{\langle 100\rangle}$ (eV)	−0.46	**−0.44**
$\Delta E_{i\text{-Fe}}^{\langle 111\rangle}$ (eV)	−0.23	**−0.24**
$\Delta E_{\text{vac-Fe}}$ (eV)	0.16	**0.14**
ΔE (eV) for $\frac{15}{16}V+\frac{1}{16}Fe=\frac{1}{16}V_{15}Fe$	−0.035	**−0.041**
ΔE (eV) for $\frac{1}{2}V+\frac{1}{2}Fe=\frac{1}{2}VFe$	−0.100	−0.447
ΔE (eV) for $\frac{1}{16}V+\frac{15}{16}Fe=\frac{1}{16}VFe_{15}$	−0.046	−0.034

N body-centered-cubic lattice sites, where one site is a vacancy and n nearest-neighbor sites of the vacancy are occupied by Fe atoms (all remaining sites are V atoms). In order to calculate the vacancy-Fe interaction energy we performed first-principles calculations using simulation cells consisting of 127 atoms (i.e., $4\times4\times4$ supercell with one vacancy), from which one V atom was replaced by one Fe atom and the internal coordinates relaxed at fixed supercell shape and volume.

Next, we studied the mixed interstitial dumbbell configurations in V in the presence of Fe impurities. We used the following definition for the interaction energy between an interstitial and Fe impurity:

$$\Delta E_{i\text{-Fe}} = E_i[1\text{Fe}] + E_p[0\text{Fe}] - E_i[0\text{Fe}] - E_p[1\text{Fe}], \quad (2)$$

where $E_i[n\text{Fe}]$ is the energy of a system containing N body-centered-cubic lattice sites, where one site is occupied by a dumbbell, one of the atoms of which is replaced by n atoms of Fe. We have performed first-principles calculations using simulation cells consisting of 129 atoms and the internal coordinates were relaxed at fixed supercell shape and volume.

III. DEVELOPMENT OF A SEMIEMPIRICAL POTENTIAL

A. Semiempirical potentials

While first-principles calculations provide an accurate and fundamental method to obtain the data necessary to describe the dynamics of defects, they are very computationally expensive to employ for large simulation cells and/or long simulation times. Similarly, *ab initio* molecular dynamics is restricted to sizes and time scales much smaller than the cascade events, which are the cause of radiation damage. Clearly, we can analyze only a very limited set of atomic configurations with a fully first-principles approach. Therefore, we follow this strategy: we perform first-principles calculations on an extensive set of atomic configurations and employ these results in the development of a set of semiempirical interatomic potentials that can be used for large-scale atomistic simulations.

In this work, we develop potentials of the Finnis-Sinclair form, the parameters of which are fitted to the first-principles data following the methodology of Refs. 21 and 26. The total potential energy is written as the sum of two contributions: a pairwise part and a local density part:

$$U = \sum_{i=1}^{N-1}\sum_{j=i+1}^{N} \varphi^{t_i t_j}(r_{ij}) + \sum_{i=1}^{N} \Phi^{t_i}(\rho_i), \quad (3)$$

where the subscripts i and j label distinct atoms, N is the number of atoms in the system, r_{ij} is the separation between atoms i and j,

$$\rho_i = \sum_j \psi^{t_i t_j}(r_{ij}), \quad (4)$$

and t_i is the element type of atom i. The binary alloy FS potential consists of eight functions, six of which can be determined using properties of the pure components. The cross functions (φ^{12} and Ψ^{12}) should be fitted to alloy properties. Note that for a single-component system the FS form coincides with the EAM form, but for a binary alloy, an EAM potential consists of seven functions, six of which describes pure components and one is the pairwise cross function.

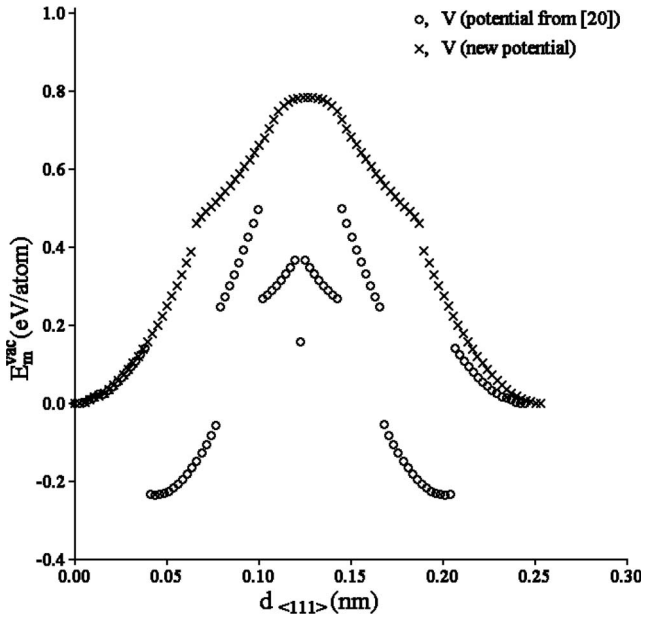

FIG. 1. Vacancy migration energy in V.

B. Semiempirical potential for pure V

A FS potential for pure Fe was developed in Ref. 21 and improved in Ref. 27. A FS potential for V was developed in Ref. 20. Some properties calculated with this potential are presented in Table I in comparison with the target values obtained from either experiment or first-principles calculation. This potential provides correct perfect crystal properties (the first five lines in Table I), and was fitted to the unrelaxed vacancy formation energy taken from first-principles data. However, it is the relaxed vacancy formation energy which is physically important, and this value is overestimated by this potential. To find the vacancy migration energy, we monitored the energy of the crystal as an atom was translated from its initial equilibrium position into an empty nearest-neighbor site (i.e., a vacancy) along a path drawn from the initial equilibrium position to its final equilibrium position (the system is relaxed at each step along this path and three atoms located far away from the migration atoms were fixed to prevent the whole cell moving). The change of energy versus distance is shown in Fig. 1. The potential from (Ref. 20) demonstrates rather complex behavior, which is probably related to the fact that there are several paths (obviously each point for this potential in Fig. 1 corresponds to one of these paths chosen by the algorithm). It is interesting that the most stable atom position in the vicinity of a vacancy is located 0.05 nm from the equilibrium lattice site. This is probably an unrealistic artifact of the fitted, semiempirical FS potential. The potential from (Ref. 20) overestimates all self-interstitial formation energies, which is not surprising since it was fitted to earlier first-principles data. This potential indicates that the ⟨111⟩ dumbbell and crowdion are the most stable self-interstitials, in agreement with the first-principles results, but the next stable self-interstitial ⟨110⟩ has an energy that is too large (with respect to first-principles calculations). This is a potential problem since this can affect self-interstitial kinetics at high temperatures (see Ref. 20 for more detailed discussion). The potential also predicts a very high melting temperature (the melting temperature was calculated using the coexistence method[28] with accuracy not worse than 5 K).

While the potential developed in Ref. 20 allowed some insight to be obtained into the self-interstitial kinetics in V, before fitting an alloy potential, it behooves us to improve the initial V potential, focusing on properly reproducing the expanded point defect formation energy data set obtained from the present first-principles calculation. In fitting the previous V potential,[20] we determined the potential parameters by the fitting to the cohesive energy and lattice parameter of the equilibrium crystalline phase, unrelaxed vacancy formation, and elastic constants. However, interstitial energies are also affected by the short-range part of the potential: MD simulations of interstitials suggest that the atomic separation near an interstitial can be compressed by 20% relative to that in the equilibrium perfect crystal. Clearly, we need to include information about atomic interactions at small atomic separations. In fitting the earlier potentials,[21,29] we found that using the universal binding energy relation is not appropriate since it does not properly distinguish between changes in density and compression of just a few bonds with only a small change in local density. To address this, we also fitted the potential to atomic forces in a liquid (where a variety of interatomic spacings occur), as determined from first-principles calculations (as originally suggested in Ref. 30). In addition, we explicitly included in the fitting procedure the formation energies of five self-interstitials. Since it is the relaxed formation energies which are important for application, the differences between energies of the perfect crystal and relaxed defect configurations were included in the fitting procedure.

The parameters for the new potential are presented in Table III. Table I demonstrates that this potential adequately describes the main properties of defects in pure V. It is especially important that it completely reproduces all interstitial formation energies. It is interesting to note that while the potential gives poor predictions for the metastable ⟨100⟩ and ⟨110⟩ dumbbell separations, it gives the correct predictions for the ground state ⟨111⟩ dumbbell separation (the dumbbell separation obtained with the FS potential is larger than the first-principles value by just 2% and the first-principles calculations underestimate the lattice parameter by 1%). The vacancy migration energy calculated with the new potential, shown in Fig. 1, appears to be much more reasonable that obtained using the FS potential from Ref. 20. The sum of the vacancy formation and migration energies gives the activation energy for self-diffusion via a vacancy mechanism. As can be seen from Table I, the new potential predicts the activation energy for self-diffusion in good agreement with low-temperature experimental data. Overall, we conclude that the new potential provides much more reliable predictions for the point defects in V than the previous V potential from Ref. 20.

C. Semiempirical potential for dilute solutions of Fe in V

Although potentials for pure ferromagnetic iron and vanadium already exist, the interactions between Fe and V in the

TABLE III. Parameters for the analytical form of the V-Fe potential (Ref. 47).

Function	Value	Cutoffs
$\varphi_{VV}(r)$	$\exp(7.0236650976148+0.38414932172994r$ $-3.9452833628150r^2+1.2044612991920r^2)$	1.0–1.7
	$-25.139133151834\ (2.2-r)^3$	1.7–2.2
	$+11.836012558032\ (2.3-r)^3$	1.7–2.3
	$-29.896310633764\ (2.4-r)^3$	1.7–2.4
	$+11.362782322594\ (2.5-r)^3$	1.7–2.5
	$-10.181574852650\ (2.6-r)^3$	1.7–2.6
	$-4.9875503863803\ (2.7-r)^3$	1.7–2.7
	$+8.6952804860732\ (2.8-r)^3$	1.7–2.8
	$-13.677500718931\ (2.9-r)^3$	1.7–2.9
	$+5.6126388727001\ (3.0-r)^3$	1.7–3.0
	$+0.46488001604193\ (3.1-r)^3$	1.7–3.1
	$+1.5214055691516\ (3.5-r)^3$	1.7–3.5
	$+0.46544307855460\ (3.9-r)^3$	1.7–3.9
	$-0.64131667364153\ (4.4-r)^3$	1.7–4.4
	$+0.14608881387672\ (4.9-r)^3$	1.7–4.9
	$+18.850648840669\ (2.7-r)^4$	1.7–2.7
$\varphi_{V\mathrm{Fe}}(r)$	$\exp(10.650423553729-8.6627918551923r$ $+3.4938728452290r^2-0.75264873240612r^3)$	1.0–2.2
	$-6.0631883671138\ (2.4-r)^3$	2.2–2.4
	$-24.799198823886\ (2.5-r)^3$	2.2–2.5
	$+26.907575069393\ (2.7-r)^3$	2.2–2.7
	$-3.0426755184804\ (2.9-r)^3$	2.2–2.9
	$+1.8009131178337\ (3.3-r)^3$	2.2–3.3
	$-1.5541857077422\ (4.1-r)^3$	2.2–4.1
	$-0.025426650046730\ (4.5-r)^3$	2.2–4.5
	$-0.40899382313291\ (4.9-r)^3$	2.2–4.9
	$+0.41143636852142\ (5.3-r)^3$	2.2–5.3
	$+49.486816355750\ (2.6-r)^4$	2.2–2.6
	$-26.949471452396\ (2.8-r)^4$	2.2–2.8
	$+0.89607791162728\ (3.1-r)^4$	2.2–3.1
	$-0.30552738676505\ (4.3-r)^4$	2.2–4.3
	$+0.92215103950722\ (4.8-r)^4$	2.2–4.8
	$-0.32653206990036\ (5.3-r)^4$	2.2–5.3
$\varphi_{\mathrm{FeFe}}(r)$	The same as in Ref. 27	
$\psi_{VV}(r)$	$4.7245287530941\ (2.4-r)^3$	0–2.4
	$+3.3757528926713\ (2.5-r)^3$	0–2.5
	$-0.84094568228487\ (2.6-r)^3$	0–2.6
	$+5.0909332213711\ (3.2-r)^3$	0–3.2
	$+0.70595885229466\ (4.0-r)^3$	0–4.0
$\psi_{V\mathrm{Fe}}(r)$	$0.51223781200262\ (2.4-r)^3$	0–2.4
	$+0.82719475666504\ (2.5-r)^3$	0–2.5
	$+3.9878638778417\ (2.7-r)^3$	0–2.7
	$+3.4726303408747\ (2.9-r)^3$	0–2.9
	$+4.5584613828918\ (3.2-r)^3$	0–3.2
	$+0.21046804631232\ (4.2-r)^3$	0–4.2
$\psi_{\mathrm{FeFe}}(r)$	The same as in Ref. 27	
$F_V(\rho)$	$-\rho^{0.5}-4.0940585433679\times10^4\ \rho^2+9.7459084965270$ $\times10^{-9}\ \rho^4$	0–∞

TABLE III. (*Continued.*)

Function	Value	Cutoffs
$F_{Fe}(\rho)$	The same as in Ref. 27	

alloy have not previously been described. In order to construct an interatomic potential to describe interactions between Fe solutes and point defects in V, two cross functions φ_{VFe} and ψ_{VFe} were developed. The parameters of these functions were fitted to some of our first-principles data. Since the goal of this work is to develop a semiempirical potential for very dilute solutions of Fe in V, we used the first-principles data (lattice parameter and formation energy) obtained on a bcc structure where one of 16 V atoms was replaced by Fe. The interaction energies between Fe and point defects [see Eqs. (1) and (2)] were included in the fitting procedure. Finally, we created a representative liquid configuration containing 120 V and 30 Fe atoms. The atomic forces determined for this configuration from the first-principles calculations were also used in the fitting procedure. In all of these configurations, the local magnetic moment on the iron atoms was found to be small. The parameters of the optimized cross-functions are provided in Table III. Figure 2 shows the effective pair potentials, defined as

$$\varphi_{\mathrm{eff}}^{t_1t_2}(r) = \varphi^{t_1t_2}(r) + \left(\left.\frac{\partial \Phi^{t_1}}{\partial \rho}\right|_{\rho_0^{t_1}} + \left.\frac{\partial \Phi^{t_2}}{\partial \rho}\right|_{\rho_0^{t_2}} \right) \psi^{t_1t_2}(r), \quad (5)$$

where the superscripts refer to the atom type and ρ_0^t is the value of ρ for atoms of type t in the equilibrium $V_{15}Fe$ lattice at $T=0$. This is a mean-field approximation to the EAM, which can be related to the alloying energy.[31,32] Since the V-Fe function is shifted to smaller atomic separations with respect to both V-V and Fe-Fe functions, we conclude that there is a strong attraction between V and Fe atoms. This is in agreement with the formation energies of V-Fe alloys being negative (see Table II). On the other hand, examination of Table II shows that the potential provides accurate predictions for dilute solutions of Fe in V and, surprisingly, for small amounts of V in Fe. Information on the latter was not included in the fitting procedure (one may appropriately have concerns about transferrability when moving from a paramagnetic to a ferromagnetic environment). There is a considerable overestimate of the absolute value of the formation energy of the $B2$ structure due to the strong nearest-neighbor attraction.

Examination of Table II shows that the new Fe-V potential yields very good agreement with most of the first-principles data on the interaction energy between Fe atoms and point defects in V. This makes this potential especially suitable for the simulation of radiation damage in (dilute) V-Fe alloys.

D. Lattice parameter and bulk modulus

There is considerable scatter in the experimental measurements of the lattice parameter of V-Fe bcc alloys (e.g., see the review in Ref. 33). Nonetheless, it is clear from the experiments that increasing Fe content leads to a decrease in the V-Fe alloy lattice parameter. Figure 3 shows the data obtained via analysis of different room-temperature experiments.[33] In order to test our potential, we created

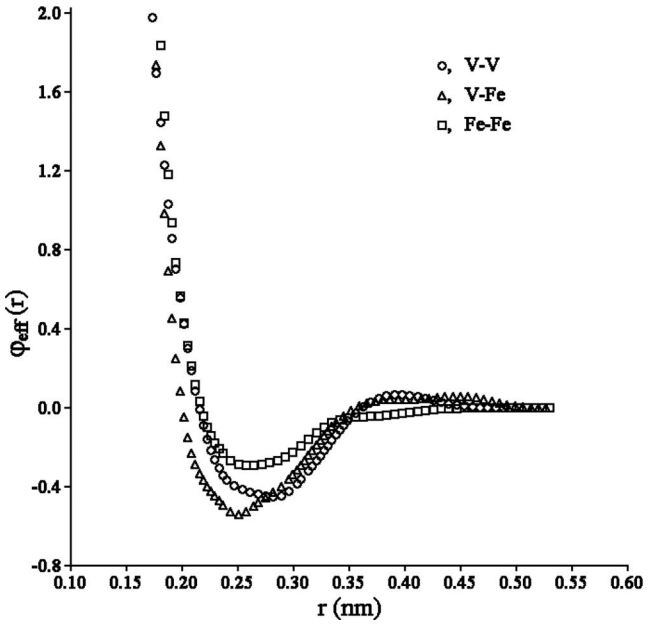

FIG. 2. Effective pair potentials.

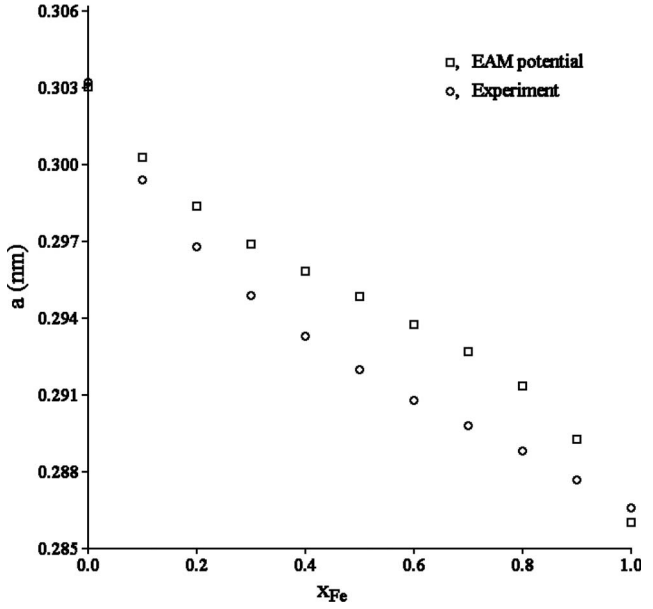

FIG. 3. Lattice parameter as a function of Fe concentration at room temperature.

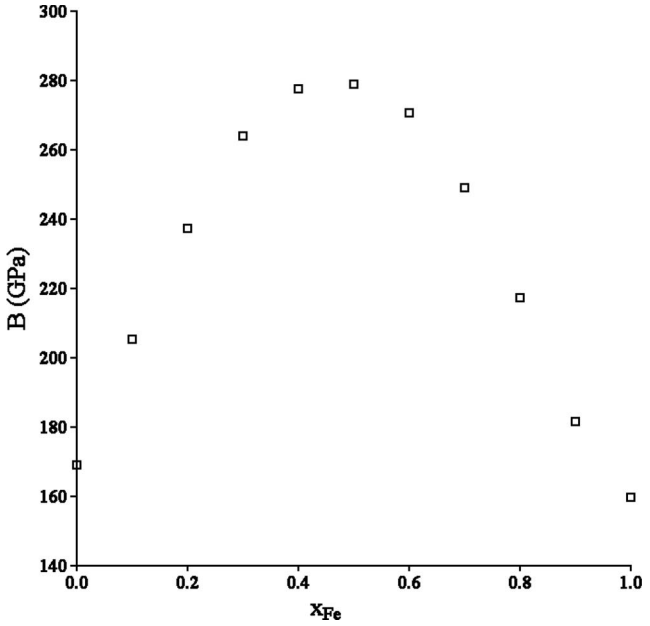

FIG. 4. Bulk modulus as a function of Fe concentration at room temperature.

model V-Fe alloys at room temperature. First, we took our model of pure V at $T=0$ consisting of 5000 atoms and randomly replaced V atoms with Fe to achieve the desired composition. Next we heated the alloys up to $T=300$ K and found the pressure as a function of the atomic density (using *NVT* molecular dynamics simulations). These calculations provided both equilibrium lattice parameters and bulk moduli. As can be seen from Fig. 3, our potential properly describes the effect of Fe on the lattice parameter at low Fe concentration. The deviation from the experimental data at $x_{Fe}=0.5$ is more pronounced.

The dependence of the bulk modulus on the Fe concentration is shown in Fig. 4. It is interesting that introduction of small quantities of Fe into V or V into Fe both increase the bulk moduli of the pure systems. (Note: no elastic constant data were used to fit the alloy cross functions in the present work.) Unfortunately, we known of no experimental data to validate our elastic modulus versus composition results. However, based on the analysis of a Finnis-Sinclair-type band filling model made in Ref. 34, we can speculate that the bulk modulus and cohesive energy contributions from the many-body term should increase as the *d* band approaches half filling, while the atomic radius should decrease with increasing *d* electron count for metals in the same row of the periodic table. The pairwise contribution to the bulk modulus will be greatest when the number of V-Fe bonds is maximized, since the V-Fe potential has the highest curvature. Alloying V in Fe or vice versa increases the modulus, so by this measure our semiempirical potential gives reasonable predictions. In order to test this qualitative picture we performed additional first-principles calculations to obtain the lattice parameters of several V-Fe compounds at $T=0$. The results are presented in Table IV. Comparison of the results of the first-principles calculations with the predictions based upon the new, semiempirical potential shows that the potential provides the correct qualitative picture, even though it greatly overestimates the first-principles elastic constants.

TABLE IV. The bulk moduli of V-Fe compounds at 0 K.

	B (GPa)	
Compound	First principles	FS potential
V (bcc)	187	156
V_3Fe ($D0_3$)	216	285
VFe (B_2)	190	398
VFe_3 ($D0_3$)	186	288
Fe (bcc)	169	178

IV. POINT DEFECT PROPERTIES IN V-Fe

Figure 5 shows the vacancy migration energy in the vicinity of a single Fe atom. In order to compare different mutual vacancy-Fe locations, all energies are calculated with respect to the state where one Fe atom is located far away from the vacancy. Therefore, the initial and final points of each curve in Fig. 5 show the vacancy-Fe binding energy. The vacancy is not bound to nearest-neighbor Fe atoms. There is, however, a very weak binding to Fe atoms at other nearby sites. This effect is largest for the Fe atom at the second-neighbor site (0.03 eV), presumably due to elastic interactions. Each peak on the curves in Fig. 5 shows a barrier for migrating atoms. The migration barriers are broadly similar, around 1 eV, with the exception of the motion of the iron atom, which is strongly suppressed. We can anticipate

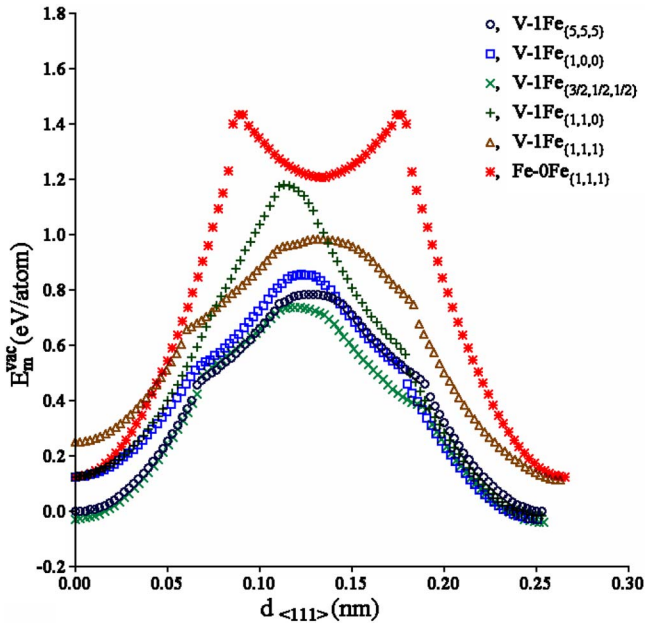

FIG. 5. (Color online) Vacancy migration energy with nearby Fe atoms. We identify each vacancy hop as A-nFe$_{\{h,k,l\}}$, where A is the type of migrating atom initially at {0,0,0} and n Fe atoms are located at position $\{h,k,l\}$ (coordinates are expressed in units of the bcc lattice parameter). The vacancy is initially at $\{1/2,1/2,1/2\}$.

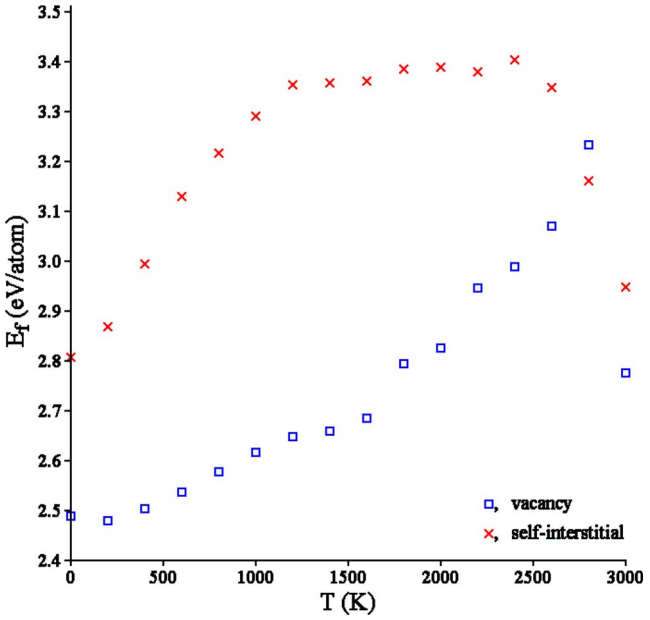

FIG. 6. (Color online) Point defect energies as a function of temperature in pure V.

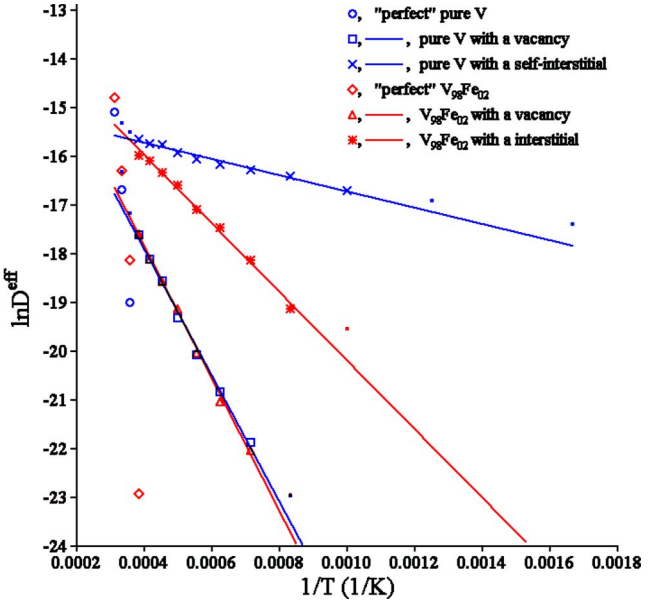

FIG. 7. (Color online) Temperature dependence of the V self-diffusivity calculated with a fixed point defect concentration (see text). The data points shown by the small symbols were excluded from the Arrhenius fit and calculation of the migration energy.

that vacancies will not be trapped by iron atoms under irradiation conditions. It is interesting to note that one of the curves shown in Fig. 5 has a double peak. The same feature was observed for several Fe potentials considered in Ref. 21.

Although calculation of static barriers along a transition path is often used to determine how point defects migrate, this approach can be incomplete because the point defect formation energies themselves may depend on temperature (e.g., see Refs. 29 and 35). The situation can be even more complicated because migration mechanisms may change with increasing temperature.[29] In order to more accurately determine diffusivities, we performed a series of molecular dynamics simulations of point defect migration at elevated temperature. First, however, we note that the V potential yields a rather high melting temperature as compared with experiment. This can lead to an underestimate of the magnitude of the changes in the vacancy formation and migration energies at elevated temperature. Nonetheless, the simulations should be able to correctly produce the main trends in the diffusivity, which are the focus of the present study.

First we determined the atomic density as function of temperature for pure V and 2% Fe solution in V. Next we performed MD relaxation of the models consisting of 2000 atoms at each temperature for 5.9 ns (in 2 fs MD time steps). Finally we introduced either one vacancy (by removing a V atom) or one interstitial (adding a single V atom). All models were first equilibrated for 40 ps and then data were collected for 5.9 ns. The model energies averaged over 5.9 ns allowed us to accurately calculate the temperature-dependent point defect formation energies (note that at a finite temperature this value is not equal to the defect formation free energy $G_f=E_f-TS_f$, where S_f is the defect formation entropy). The results for pure V are shown in Fig. 6. The vacancy formation energy increases with temperatures up to $T=2800$ K and then suddenly drops. The increase of the vacancy formation with temperature is not unusual; similar results were found for pure Al (Ref.35) and Zr.[29] The interstitial formation energy is more complex; as the temperature is raised, it first increases, then plateaus between 1000 and 2600 K and then drops sharply.

The diffusivity can be determined directly from the MD simulations in terms of the mean square displacement of atoms $\langle \Delta r^2 \rangle$,

$$D = \frac{\langle \Delta r^2 \rangle}{6t}, \tag{6}$$

where t is the simulation time over which the mean square displacement is averaged. It is interesting that atoms can diffuse even in a "perfect" bcc lattice (i.e., one in which no point defects were introduced) close to the melting temperature (see Figs. 7 and 8). We refer to this as the intrinsic mechanism of diffusion. This mechanism was also observed for Zr,[29] which is also bcc at high temperature. Of course the activation energy for such a diffusion mechanism is extremely high (see Table V) such that it makes a significant contribution to the diffusivity only near the melting temperature. The intrinsic mechanism of diffusion is likely associated with the production of Frenkel pairs. Insofar as we are aware, significant intrinsic diffusion has not been observed in either fcc and hcp metals. Because of the existence of this intrinsic mechanism, we exclude for the high-temperature data (where intrinsic diffusion is significant) from our determination of the activation energy for point-defect-based diffusion.

Figure 7 shows the V self-diffusion data in the models containing either one vacancy or interstitial. Except for high temperatures (where the intrinsic mechanism of diffusion becomes important) and low temperatures (where diffusion is too slow to yield sufficient statistics from the MD simula-

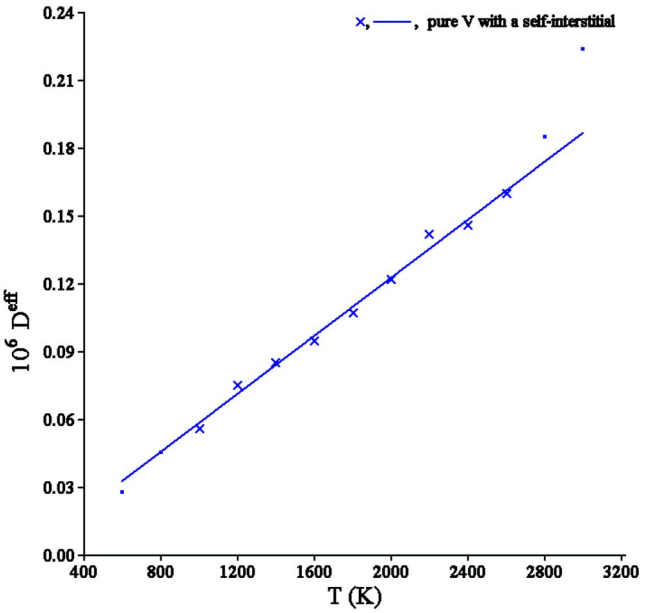

FIG. 8. (Color online) Temperature dependence of the V self-diffusivity in the interstitial mechanism.

tions), the data were well fitted by an Arrhenius expression. Since the point defect concentration was the same at all temperatures, the slopes of the Arrhenius plots are the vacancy and interstitial migration energies (divided by the Boltzmann constant). These values are shown in Table V. It is interesting that the vacancy migration energy appears to be larger than the barrier obtained from static calculation. The interstitial migration energy is much smaller than the vacancy migration energy, while interstitial formation energy is higher than the vacancy formation energy. Thus under thermal conditions, self-diffusion in pure V proceeds via the vacancy mechanism at low temperatures and via the interstitial mechanism at high temperatures, where the transition is at ~1200 K. Note that, in our analysis, we ignored the effect of the entropy part of the activation free energy.

The additional increase in the activation energy observed in experiment at high temperature may be associated with the contribution of the intrinsic mechanism of self-diffusion, as discussed above. Under irradiation conditions, similar numbers of vacancies and interstitials are produced athermally. In such cases, defect formation energies are irrelevant and diffusion will be dominated by interstitials at all temperatures.

TABLE V. Point defect migration energies inferred from MD diffusivity calculations.

Diffusant	Matrix	Point defect	E_m^{vac} (eV/atom)
V	Pure V	None	7.56
V	Pure V	Vacancy	1.12
V	Pure V	Interstitial	0.14
V	$V_{98}Fe_{02}$	None	6.44
V	$V_{98}Fe_{02}$	Vacancy	1.18
V	$V_{98}Fe_{02}$	Interstitial	*0.61*
Fe	$V_{98}Fe_{02}$	None	6.07
Fe	$V_{98}Fe_{02}$	Vacancy	0.94
Fe	$V_{98}Fe_{02}$	Interstital	0.04

While our simulations focus on high temperatures, an earlier simulation study[36] examined self-interstitial diffusion in pure V starting from $T=100$ K. In that study, the authors found that the diffusivity data do not lie on a straight line in Arrhenius coordinates and a sharp change in the slope was observed around $T=700$ K. This effect was attributed to the rotation of the self-interstitial between ⟨111⟩ directions via a barrier at ⟨110⟩. These results do not contradict our data since we consider diffusion only starting from $T=600$ K and data at $T \geqslant 1000$ K were used to determine the migration energy. We anticipate that for the new potential the transition associated with the self-interstitial rotation will occur at lower temperature since the new potential yields a difference between the ⟨110⟩ and ⟨111⟩ self-interstitial formation energies of 0.28 eV (in accordance with the first-principles data) vs 0.46 eV found from the potential used in Ref. 36. The migration barrier of the ⟨111⟩ crowdion is 0.02 in each case. The authors of Ref. 36 correctly note that when the migration energy is smaller than kT, diffusion is not thermally activated (i.e., it is athermal). Indeed our data for the self-diffusivity in the interstitial mechanism also fall on the straight line in the D vs T coordinates as was suggested in Ref. 36 (see Fig. 8).

We now consider the effect of Fe on point defects in V. Figure 7 shows that the addition of Fe accelerates V diffusion via the intrinsic mechanism. This may be associated with two facts: (i) Fe decreases the melting temperature of V and (ii) Fe has a smaller atomic radius than V (leading to smaller migration barriers). Since Fe is repelled from vacancies, it does not significantly affect vacancy diffusion, as seen in Fig. 7 and Table V. However, since Fe is attracted to interstitials, addition of Fe dramatically decreases the V diffusion via the interstitial mechanism (see Fig. 7). The apparent fourfold increase of the V migration energy in the interstitial mechanism is due not to a real increase in barrier energy, rather it shows that the interstitial spends most of its time associated with Fe, enhancing Fe diffusion and reducing V self-diffusion. Interstitial diffusion in pure vanadium is especially fast on account of the possibility of multiple correlated jumps for 1D migration along ⟨111⟩. The iron impurities disrupt this motion in two ways, first by direct pinning of the ⟨111⟩ interstitial if the Fe lies in the path of the interstitial, and second by forcing the ⟨111⟩ dumbbells to reorient away from the fast ⟨111⟩ direction into the slower ⟨110⟩ direction. This rotation restores the Arrhenius behavior.

Figure 9 shows the results of the simulation for Fe diffusion. Of course, these data contain more noise since the models contained only 40 Fe atoms. However, the trends are quite clear. Fe atoms diffuse faster than V atoms via the intrinsic mechanism. The diffusivities of the Fe and V atoms in the V-rich alloy via the vacancy mechanism are very similar. Finally, Fe atoms diffuse very much faster than V atoms in the V-rich alloy via the interstitial mechanism; the Fe migration energy is very low and the Fe diffuses athermally. Tables I and II show that the lowest mixed interstitial formation energy (which is the sum of the self-interstitial formation energy and the self-interstitial–substitutional interaction energy) at $T=0$ is $2.81-0.24=2.57$ eV. This value is just a

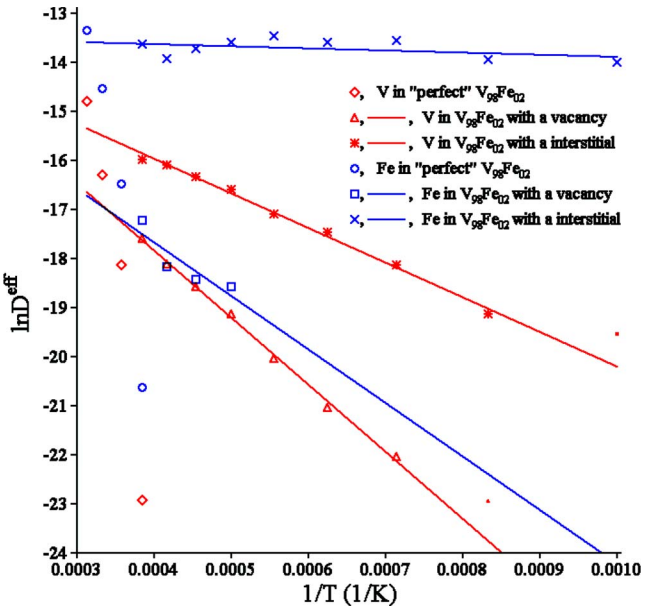

FIG. 9. (Color online) Temperature dependence of the Fe diffusivity in V calculated under the condition of a fixed defect concentration (see text). The data points shown by small symbols were excluded from the Arrhenius fit calculation of the migration energy.

little smaller than the energy of formation of the vacancy-Fe pair, which is 2.49+0.14=2.63 eV. Since the Fe migration barrier in the vacancy mechanism is much higher than that in the interstitial mechanism, this is consistent with our MD result that Fe diffuses in V via an interstitial mechanism.

V. CONCLUSIONS

To summarize, we have performed a series of first-principles point defect calculations in vanadium with and without small amounts of iron to expand the existing point defect data base. We have introduced an electronic structure embedding approach to improve the description of point defects by including semicore electrons for some V atoms (those near to the interstitial where the semicore levels are broadened) but not those further from the point defect. This enables us to combine good accuracy at the defect with large supercells to correctly describe the short-range electronic effects and the long-range strain fields. Our first-principles calculations show that vacancies are not attracted to Fe impurities, but that interstitials are, and the configuration of the interstitial can be changed from ⟨111⟩ to ⟨110⟩ by the presence of Fe.

Based on these data, previous first-principles work, and new calculations of model liquid structures, we have fitted an interatomic potential for the V-Fe system that describes the important configurations likely to arise when such alloys are exposed to neutron radiation. This potential is in a form suitable for molecular dynamics simulations of large systems.

Using the potential, we have calculated the migration barriers of vacancies in the presence of iron, showing that these are broadly similar, and that iron and vacancies do not comigrate, but that iron migration is greatly enhanced by the presence of interstitials. Vanadium self-diffusion via an interstitial mechanism is dramatically slowed by the presence of small quantities of iron, which traps and rotates the dumbbell interstitial. Escape from the pinned configuration becomes the barrier to this mechanism. It is not clear how or even whether this is connected with the dramatic increase in irradiation swelling observed when Fe is added to vanadium.[14,15]

Although the trends are the same, there is a marked numerical discrepancy in each case between migration barriers calculated from molecular dynamics and those evaluated from static barrier calculations. Since this appears in the exponent of the diffusion rate, it suggests that simply employing static migration barriers in, for example, a kinetic Monte Carlo approach, may give aging processes in error by an order of magnitude.

Although the focus of this study has been Fe in V, it illustrates the dramatic effects that even a small amount of alloying material can have on diffusion properties. While we have concentrated on the dilute iron limit here, it is likely that at higher concentrations other considerations, such as migration of interstitial clusters with multiple Fe atoms, may become important.

ACKNOWLEDGMENTS

Work at the Ames Laboratory was supported by the Department of Energy, Office of Basic Energy Sciences, under Contract No. DE-AC02-07CH11358. Work at Edinburgh was supported by EPSRC under Grant No. S81186 and the European Union under the PERFECT project. This work was also supported by Department of Energy, Office of Fusion Energy Sciences (Contract No. DE-FG02-01ER54628).

[1] H. Nakajima, S. Yoshida, Y. Kohno, and H. Matsui, J. Nucl. Mater. **191**, 952 (1992).
[2] F. A. Garner, D. S. Gelles, H. Takahashi, S. Ohnuki, H. Kinoshita, and B. A. Loomis, J. Nucl. Mater. **191**, 948 (1992).
[3] K. Fukumoto, H. Matsui, Y. Candra, K. Takahashi, H. Sasanuma, S. Nagata, and K. Takahiro, J. Nucl. Mater. **283**, 535 (2000).
[4] H. Tsai, T. S. Bray, H. Matsui, M. L. Grossbeck, K. Fukumoto, J. Gazda, M. C. Billone, and D. L. Smith, J. Nucl. Mater. **283**, 362 (2000).
[5] N. Nita, T. Iwai, K. Fukumoto, and H. Matsui, J. Nucl. Mater. **283**, 291 (2000).
[6] T. Hayashi, K. Fukumoto, and H. Matsui, J. Nucl. Mater. **283**, 234 (2000).
[7] R. J. Kurts, K. Abe, V. M. Chernov, V. A. Kazakov, G. E. Lucas, H. Matsui, T. Muroga, G. R. Odette, D. L. Smith, and S. J. Zinkle, J. Nucl. Mater. **283**, 70 (2000).
[8] T. Hayashi, K. Fukumoto, and H. Matsui, J. Nucl. Mater. **307**, 930 (2002).

[9] T. Muroga, T. Nagasaka, K. Abe, V. M. Chernov, H. Matsui, D. L. Smith, Z. Y. Xu, and S. J. Zinkle, J. Nucl. Mater. **307**, 547 (2002).
[10] N. Nita, T. Yamamoto, T. Iwai, K. Yasunaga, K. Fukumoto, and H. Matsui, J. Nucl. Mater. **307**, 398 (2002).
[11] N. Nita and H. Matsui, Mater. Trans. **46**, 522 (2005).
[12] K. Fukumoto, H. Matsui, T. Muroga, S. J. Zinkle, D. T. Hoelzer, and L. L. Snead, J. Nucl. Mater. **329**, 472 (2004).
[13] S. Konishi, A. Kimura, M. Akiba, H. Nakamura, T. Nagasaka, T. Muroga, A. Hasegawa, and H. Matsui, Nihon Genshiryoku Gakkaishi **46**, 311 (2004) [J. Atomic Energy Soc. Jpn. **46**, 311 (2004)].
[14] B. A. Loomis, D. L. Smith, and F. A. Garner, J. Nucl. Mater. **179**, 771 (1991).
[15] K. Fukumoto, A. Kimura, and H. Matsui, J. Nucl. Mater. **258**, 1431 (1998).
[16] H. M. Chung, B. A. Loomis, and D. L. Smith, J. Nucl. Mater. **239**, 139 (1996).
[17] H. Matsui, H. Nakajima, and S. Yoshida, J. Nucl. Mater. **205**, 452 (1993).
[18] M. S. Daw and M. I. Baskes, Phys. Rev. B **29**, 6443 (1984).
[19] M. W. Finnis and J. E. Sinclair, Philos. Mag. A **50**, 45 (1984).
[20] S. Han, L. A. Zapeda-Ruiz, G. J. Ackland, R. Car, and D. J. Srolovitz, J. Appl. Phys. **93**, 3328 (2003).
[21] M. I. Mendelev, S. Han, D. J. Srolovitz, G. J. Ackland, D. Y. Sun, and M. Asta, Philos. Mag. A **83**, 3977 (2003).
[22] J. P. Perdew, K. Burke, and M. Ernzerhof, Phys. Rev. Lett. **77**, 3865 (1996).
[23] G. Kresse and J. Hafner, Phys. Rev. B **47**, R558 (1993); **49**, 14251 (1994).
[24] S. Baroni *et al.*, http://www.pwscf.org
[25] D. Vanderbilt, Phys. Rev. B **43**, 6796 (1991).
[26] M. I. Mendelev, D. J. Srolovitz, G. J. Ackland, and S. Han, J. Mater. Res. **20**, 208 (2005).
[27] G. J. Ackland, M. I. Mendelev, D. J. Srolovitz, S. Han, and A. V. Barashev, J. Phys.: Condens. Matter **16**, S2629 (2004).
[28] J. R. Morris, C. Z. Wang, K. M. Ho, and C. T. Chan, Phys. Rev. B **49**, 3109 (1994).
[29] M. I. Mendelev and G. J. Ackland, Philos. Mag. Lett. **87**, 349 (2007).
[30] F. Ercolessi and J. B. Adams, Europhys. Lett. **26**, 583 (1994).
[31] G. J. Ackland and V. Vitek, Phys. Rev. B **41**, 10324 (1990).
[32] G. J. Ackland and V. Vitek, Philos. Mag. B **62**, 149 (1990).
[33] J. F. Smith, Bull. Alloy Phase Diagrams **5**, 184 (1984).
[34] G. J. Ackland and S. K. Reed, Phys. Rev. B **67**, 174108 (2003).
[35] M. I. Mendelev and B. S. Bokstein, Mater. Lett. **61**, 2911 (2007).
[36] L. A. Zepeda-Ruiz, J. Rottler, S. Han, G. J. Ackland, R. Car, and D. J. Srolovitz, Phys. Rev. B **70**, 060102(R) (2004).
[37] W. B. Pearson, *Handbook of Lattice Spacings and Structures of Metals and Alloys* (Pergamon Press, Oxford, 1967).
[38] C. Kittel, *Introduction to Solid State Physics* (Wiley, New York, 1986).
[39] G. Simmons and H. Wang, *Single Crystal Elastic Constants and Calculated Aggregate Properties: A Handbook* (MIT Press, Cambridge, MA, 1971).
[40] First-principles calculations performed as part of this work.
[41] I. S. Grigorev and E. Z. Meilihova, *Fizicheskie Velichiny* (Energoatomizdat, Moscow, 1991) (in Russian).
[42] The data for the temperature interval from 1150 to 1600 K (Ref. 41).
[43] The data for the temperature interval from 1600 to 2100 K (Ref. 41).
[44] A. I. Efimov, L. P. Belorukova, I. V. Vasilkova, and V. P. Chechev, *Svoistva Neorganicheskih Soedinenii* (Himiia, Leningrad, 1983) (in Russian).
[45] The self-interstitial formation energies were fitted to earlier first-principles data (see the text).
[46] The target values for the lattice parameters were obtained by the rescaling of the first-principles data to take into account that the first-principles calculations underestimate the V lattice parameter by 1% and the EAM potential for V was fitted to the experimental lattice parameter.
[47] All distances are expressed in Å and energies in eV. The two numbers listed as "cutoff" indicate the range of the adjacent basis function: a function with cutoff $x-y$ should be multiplied by $H(r-x)H(y-r)$ where H is the Heaviside step function. The potential functions are available in a tabulated format at http://lammps.sandia.gov